MINIREVIEW

Check for updates

Recent advances in plasmonic Prussian blue-based SERS nanotags for biological application

Ya-Qin Liu,[a] Wei Zhu,*[b] Ji-Ming Hu[a] and Ai-Guo Shen [ID] *[b]

The reliability and reproducibility of surface-enhanced Raman scattering (SERS) technology is still a great challenge in bio-related analysis. Prussian blue (PB)-based SERS tags have attracted increasing interest for improving these deficiencies due to its unique Raman band (near 2156 cm^{-1}) in the Raman-silent region, providing zero-background bio-Raman labels without interference from endogenous biomolecules. Moreover, the stable PB shell consisting of multiple layers of CN^{-} reporters ensure a stable and strong Raman signal output, avoiding the desorption of the Raman reporter from the plasmonic region by the competitive adsorption of the analyte. More importantly, they possess outstanding multiplexing potential in biological analysis owing to the adjustable Raman shift with unique narrow spectral widths. Despite more attention having been attracted to the structure and preparation of PB-based SERS tags for their better biological applications over the past five years, there is still a great challenge for SERS suitable for applications in the actual environment. The biological applications of PB-based SERS tags are comprehensively recounted in this minireview, mainly focusing on quantification analysis, multiple-spectral analysis and cell-imaging joint phototherapy. The prospects of PB-based SERS tags in clinical diagnosis and treatment are also discussed. This review aims to draw attention to the importance of SERS tags and provide a reference for the design and application of PB-based SERS tags in future bio-applications.

1. Introduction

Since the surface-enhanced Raman scattering (SERS) phenomenon was first confirmed to perform the great capacity of improvement in the sensitivity of Raman spectroscopy in the 1970s,[1–3] the million-fold enhancement of the Raman signal on metal surfaces, and even the detection at the single-molecule level has been achieved by SERS.[4–6] In the past few decades, SERS has been demonstrated in numerous important applications in various fields, such as material sciences,[7,8] analytical chemistry,[9–11] physical chemistry,[12,13] and biomedical research.[2,14,15] Admittedly, SERS has become an ideal alternative for biological analysis because of its inherent advantages, including the weak Raman signal of water, fingerprinting capabilities, ultra-sensitivity, high specificity, resistance to photobleaching and photodegradation.[16,17]

In general, SERS biological analysis can be classified into direct (label-free)[18–20] and indirect (labelled) SERS detection.[21–23] Direct SERS detection depends on capturing bio-analytes in the plasmonic region, thus acquiring the fingerprint information of bio-analyte. However, it is limited in the biosystem due to the lack of standard SERS spectra for numerous biomolecules, complicated analysis of Raman peaks and complex biological environments. In contrast, indirect SERS detection relies on the Raman signals provided by SERS tags, circumventing the toilsome analysis of Raman spectra and providing a strategy to study some physical properties in the biosystem, which are impossible to be reflected directly by inherently related molecules. Thus, indirect SERS detection has been widely applied to monitor the dynamic changes in biomolecules[24,25] and intracellular environment properties.[26,27] Notably, the SERS tag plays a vital role in indirect SERS detection,[28,29] consisting of an enhanced substrate, Raman reporters and targeting molecules. The commonly-used Raman reporters are shown in Table 1, including some nitrogen-containing cationic dyes,[30,31] sulfur-containing dyes,[32,33] thiol-small molecules[34–36] and triple-bond-containing molecules.[37,38] These Raman reporters have contributed to the preeminent SERS application in life sciences by binding with the enhanced substrates through the electrostatic forces or S–Au(Ag) interactions. Nevertheless, these Raman reporters can fall off due to the competitive adsorption of the analyte on the metal surface, resulting in unstable Raman signals. Although protection strategies with a carbon shell[39] or polymers[40] have been proposed to avoid the desorption of the Raman reporters, they are still limited due to the strict synthesis process of the protective shell, the biocompatibility, the background signal interference and the production efficiency of the

[a]*College of Chemistry and Molecular Sciences, Wuhan University, Wuhan 430072, China*

[b]*School of Printing and Packaging, Wuhan University, Wuhan 430079, China. E-mail: zwmaterials@whu.edu.cn; agshen@whu.edu.cn*

Table 1 The commonly-used Raman reporters for the preparation of SERS nanotags

Type	Example	Specific Raman scattering	Linking mode	Ref.
Traditional Raman reporters	Crystal violet	Fingerprint region (400–1800 cm^{-1})	Electrostatic force	30 and 41
	3,3′-Diethylthiadicarbocyanine iodide		S–Au(Ag) interaction	32 and 33
	4-Methylbenzenethiol			36 and 42
Triple-bond containing Raman reporters	4-Mercaptobenzonitrile	Raman silent region (1800–2800 cm^{-1})	S–Au(Ag) interaction	43 and 44
	4-Ethynylbenzenethiol derivatives			37

hot spots. Therefore, effective Raman reporters are still a key to improving the sensitivity and stability of the indirect SERS detection.

Prussian Blue (PB), a dark blue pigment discovered in the 1706s, has been demonstrated as a promising coordination polymer as the Raman reporter with the formula of $Fe_4^{III}[Fe^{II}(CN)_6]_3 \cdot nH_2O$.[45–47] Interestingly, it was discovered that PB only possesses a strong and sharp Raman peak in the Raman-silent region (1800–2800 cm^{-1}), where the Raman signal interference of biological endogenous molecules is effectively circumvented.[48,49] Based on the unique characteristics of PB, Liu's group achieved a high-sensitivity immunoassay for antigen detection with the limit of detection (LOD) of 8.0 fg mL^{-1} using a PB-based SERS tag.[50] Background-free cancer cell imaging has also been achieved by them. They demonstrated the potential of PB as a high signal-to-background ratio (SBR) and zero-background resonant Raman reporter. Since then, the unique Raman scattering of PB and its analogues (PBA) have made them rising stars in optical labels with the properties of ultra-sensitivity, super-stability, and high-specificity. Recently, PB-based SERS tags with different morphologies have been successfully prepared for indirect SERS detection and imaging in biological systems. The wide application of the PB-based SERS tags will facilitate the investigation of complex intracellular biological events without the interference of endogenous signals and provide new possibilities for precise disease diagnosis.

In this review, we give a detailed discussion on the most recent advances of PB-based SERS tags. At first, we will emphatically discuss the rational design of the PB-based SERS tag to provide credible guidance for extending the biological application of the PB-based SERS tag. Secondly, the applications of PB-based SERS tags in the biological field will be summarized, such as the monitoring of the intracellular environment, tumour imaging, bacterial coding and cancer cell classification (Fig. 1). Finally, the challenges and the prospects of PB-based SERS tags in biological applications are also discussed.

2. Rational design of PB-based SERS tags for bioanalysis

The SERS tags are usually the first-mentioned part in the indirect SERS detection, generally consisting of a SERS-enhanced substrate, Raman reporters and targeting biomolecules[28,51] (Fig. 2A). Protection shells are also introduced into some SERS tags to obtain a more stable Raman signal output. Constructing

PB-based SERS tags should take the following principles into account: (1) a proper metal nanostructure will provide strongly enhanced Raman signals because of the local surface plasmonic resonance (LSPR) on the metal surface,[1,52] which lays a solid foundation for SERS tags. The SERS properties of the tags can also be greatly affected by the chemical composition,[53,54] size,[55,56] and structure of the enhanced substrate.[57,58] (2) In general, the Raman reporters are required to attach to the surface of a SERS-enhanced substrate because the most widely accepted mechanisms, electromagnetic enhancement (EM) and chemical enhancement (CE), are strongly distance-dependent or chemical bonding-dependent, respectively. In addition, a strong interaction between the Raman reporters and substrate is indispensable for preventing reporter desorption during further modification or use. (3) A dense, uniform Raman reporter layer formed on the substrates will contribute to a strong and stable signal. (4) Furthermore, the detection specificity in bioanalysis is decided by the biorecognition element, e.g. aptamer, which is used to target the analyte.
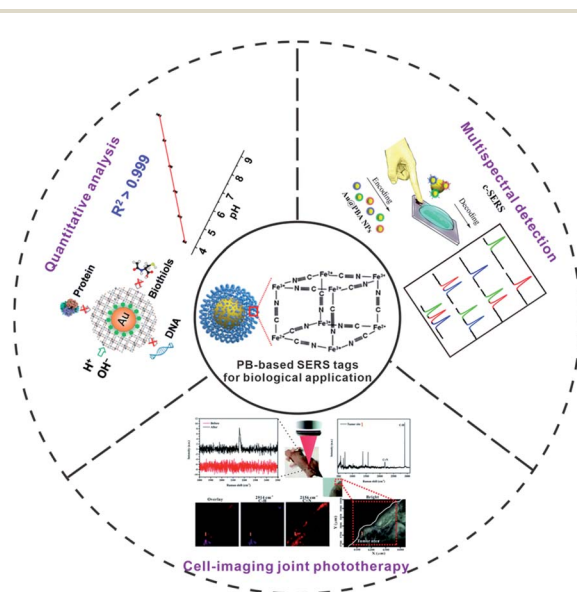

Fig. 1 Multifunctional PB-based SERS tags used for biological applications. PB-based SERS nanotags for quantitative analysis, adapted from ref. 88 with permission from American Chemical Society. Copyright 2020 American Chemical Society. Multispectral detection, adapted from ref. 89 with permission from American Chemical Society. Copyright 2020 American Chemical Society. Cell-imaging joint phototherapy, adapted from ref. 65 with permission from Royal Society of Chemistry. Copyright 2020 Royal Society of Chemistry.
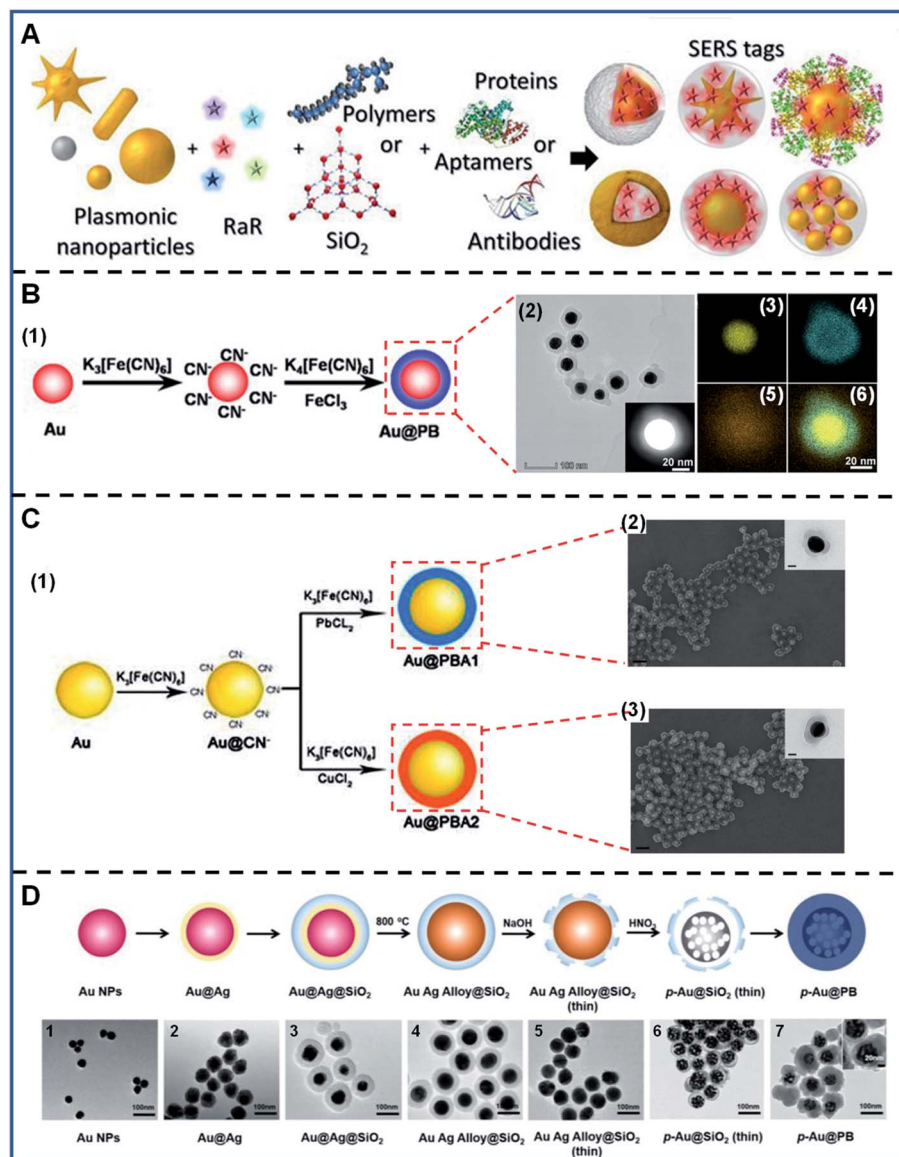
Fig. 2 The basic constituents of SERS tags and the synthesis of PB-based nanomaterials. (A) The representation of the basic elements of SERS tags. Adapted with permission from ref. 51. Copyright 2019 American Chemical Society. (B) The synthesis and characterization of Au@PB NPs: (B.1) A schematic illustrating the synthesis of Au@PB NPs; (B.2) TEM images, the inset is the corresponding high-angle annular darkfield scanning TEM image; (B.3–B.6) EDX mapping of Au, Fe, O and the overlay images. Reproduced with permission from ref. 61. Copyright 2021 American Chemical Society. (C) The synthesis and characterization of Au@PBA NPs: (C.1) Schematic illustrating the synthesis procedure of Au@PBA NPs; (C.2) SEM image of Au@PBA (Cu) NPs, the inset is the TEM image of a single Au@PBA (Cu) NP; (C.3) SEM image of Au@PBA (Pb) NPs, the inset is the TEM image of a single Au@PBA (Pb) NP. Reproduced with permission from ref. 62. Copyright 2021 Elsevier. (D) The synthesis and characterization of p-Au@PB NPs: (D.1–D.7) TEM images of the formed process of p-Au@PB NPs, the inset is the magnified image of p-Au@PB NPs. Adapted with permission from ref. 63. Copyright 2019 John Wiley & Sons, Inc.

2.1. Component of PB-based SERS tags

PB-based SERS tags can be simply divided into two parts: one is PB-based nanomaterials, another is targeting molecules. To date, the PB-based nanomaterials commonly comprise the gold (Au) nanosphere as the core and the PB or the PBA as the shell. Au nanoparticles (Au NPs) are the most widely used enhanced substrate for PB-based SERS tags in biological applications due to their established synthetic methods, super excellent biocompatibility and low toxicity. Although silver is recommended as the most efficient plasmonic metal, it is unsuitable for PB-based SERS tags due to its extreme instability caused by the etching of CN^- and the toxicity to living systems.[59,60] In addition, the spherical particle is relatively easy to control during the fabrication and has better long-term stability. Meanwhile, the PB or PBA shell as the Raman reporter can provide a single stable signal output in the bio-silent region. The core–shell nanostructure ensures the strong Raman signal of PB-based nanomaterials, effectively circumventing the desorption of the Raman reporter caused by the competitive adsorption of the analyte.
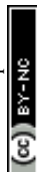
Apart from spherical Au NPs as the core, another attempt has also been made for the fabrication of porous gold (p-Au) NPs as the core. PB-coated p-Au NPs with abundant Raman hot spots have been put forward by Liu's group to amplify the Raman signals of the PB shell. PB is not only used as the Raman reporter but can also be used as the protective shell for other Raman reporters. For instance, PB-caged 4-mercaptopyridine (4-MPy)-Au NPs have been successfully synthesized by Liu's group, in which the PB shell is both used as the internal standard and a cage-like protective layer, as well as a carrier that only allows the entry of H^+ or OH^-.

2.2. Preparation and advantages of PB-based nanomaterials

2.2.1. Preparation of PB-based nanomaterials. With the development of nanomaterial preparation technology, a facile method has been fully developed for preparing PB-based nanomaterials, laying a rigid foundation for the better bio-applications of PB-based SERS tags. Briefly, spherical Au NPs with uniform size have been synthesized through classic sodium citrate reduction at the beginning. The size of Au NPs can be controlled by adjusting the dosage of sodium citrate and $HAuCl_4$. The most used size of Au in PB-based nanomaterials to obtain high electromagnetic enhancement and maintain the long-term stability of NPs is 50 ± 10 nm. The coating process of PB or PBA shell involves two simple steps[61,62] (Fig. 2B and C). One is the synthesis of CN-etched Au NPs, which is also called Au@CN NPs. In this step, Au NPs are etched by the added $K_3[Fe(CN)_6]$ solution. The etching time is important because too long an etching time will result in the instability of the nanoparticles, and too short an etching time is not conducive to the formation of the Pb shell. The other step is the addition of PB precursors, including $K_4[Fe(CN)_6]$ solution and $FeCl_3$ solution for forming the PB shell, $K_4[Fe(CN)_6]$ solution and $PbCl_2$ or $CuCl_2$ for forming the PBA shell. The thickness of the PB or PBA shell can be controlled by adjusting the addition rate and the concentration of PB precursors. Besides, the addition rate of the precursor is required to be finely controlled to guarantee the growth of the PB or PBA shell on the Au core surface rather than nucleating independently in solution. The synthesis of p-Au@PB NPs as mentioned in Section 2.1 is more complicated for obtaining the porous gold structure, as shown in Fig. 2D.[63].

2.2.2. Advantages of PB-based nanomaterials for bio-analysis. In the PB-based nanomaterials, PB and PBA are regarded as the Raman reporters to produce the unique Raman signal. Compared with the commonly used Raman reporter molecules, using PB or PBA as the Raman reporter has many merits: (1) the large Raman scattering cross-section of PB and PBA endows them with strong Raman signals, and Au@PB NPs will produce a stronger Raman signal due to the production of surface-enhanced resonance Raman scattering in the presence of the 633 nm and 785 nm lasers. (2) The unique Raman scattering of PB and PBA in the bio-silent zone eliminates the interference of endogenous molecules in the biosystems. (3) The core–shell nanostructure ensures the close integration between PB or PBA and the enhanced substrate, solving the possible desorption of the commonly used Raman reporters

when there is no protection shell. More importantly, protective shells are usually indispensable in preventing the falling off of the traditional Raman reporters, which may weaken the enhanced effect of SERS due to the thickness of the protected shells. In PB-SERS nanotags, the PB shell can not only be seen as an effective Raman reporter but it can also be used as a Raman-active protective shell, simplifying the synthesis process and improving the detection sensitivity and reproducibility.

2.3. Specific targeting of analytes

The recognition of PB-based SERS tags toward a specific cellular region or specific molecule in the biosystem is typically attained with the specific targeting ligands, which generally consist of specific proteins, peptides, aptamers, polysaccharides, or antibodies. For instance, some proteins or peptides containing free sulfhydryl groups, such as ovalbumin, were coated on the NPs due to the inherent capacity of proteins to attach to the NPs via S–Au bonds.[64] Stable covalent bonds between the aptamers[62] or polysaccharides[65] and the PB-based nanomaterials can also be formed with the aid of poly-L-lysine (PLL) as a bridge, the 1-ethyl-3-(3-dimethylaminopropyl) carbodiimide (EDC) and N-hydroxysuccinimides (NHS) as the coupling reagent. The activated PLL by EDC and NHS provides abundant amine moieties to react with the carboxylic acid groups in the aptamers or polysaccharides. Similarly, the positively charged PLL is also used as the bridge for the connection of the PB-based nanomaterials and the negative antibody[50] by electrostatic adsorption. In addition, some special molecules, e.g., folic acid (FAs)[63] receptors, are overexpressed in various cancer cells, thus FAs can be treated as the specific targeting ligands. Even though the functional PB-based nanomaterials through specific bio-recognition molecules have been widely used as SERS tags for both in vitro and in vivo cell targeting and imaging, a variety of bio-applications are still constantly emerging.

3. Biological applications of Prussian blue-based SERS nanotags

Many organic molecules, such as proteins,[66,67] DNA,[68,69] and metabolites,[70,71] perform essential functions in multiple biological processes, including signal transduction, cell adhesion and migration, metabolism, etc. The visible spatial distributions and reliable quantification detection of these important molecules present in biological systems provide solid foundations to further understand their important function and will drive advances in various fields such as early disease diagnostics. Moreover, the intracellular environment is also a critical physiological parameter that is an indicator to reveal the abnormal phenomenon in vivo.[72,73] The comprehensive detection and imaging of these endogenous molecules have attracted more and more attention with the increased rate of various diseases. PB-based SERS tags are particularly helpful for long-term imaging applications in biosystems due to their ability to resist photobleaching and photodegradation, which overcomes the shortcoming of fluorophore labels. Furthermore, the low cytotoxicity of SERS tags is the prerequisite to enter the cell,

increasing the requirements for the selection of the enhanced substrate and the Raman reporter. Taking this into account, PB-based SERS tags exhibit powerful advantages because PB was allowed to be an antidote for the treatment of thallium and cesium intoxication by the Food and Drug Administration (FDA) in 2003, showing the outstanding biocompatibility of PB. We present below some typical examples that elaborate the current interest in using PB-based SERS tags, as compared to previously reported methods.

3.1. Reliable SERS quantitative analysis

Signal reproducibility of SERS tags is decisive for reliable quantitative SERS bioanalysis. Quantitative SERS analysis is by far plagued due to the uneven distribution of hot spots on SERS-enhanced substrates and the possible desorption of Raman reporters. The environmental conditions also have a crucial impact and can cause the fluctuation of the Raman signal. Various attempts, such as protective coating,[29,74] internal standards[75,76] and ratiometric SERS[77,78] assays, have been carried out to alleviate the present dilemma in quantitative SERS analysis techniques. The introduction of a protective coating effectively avoids the leaching of Raman reporter molecules and prevents potential signal fluctuation caused by the surrounding medium. However, the increased shell thickness probably results in a decrease in the detection sensitivity due to the distance dependence of EM, and the complex synthesis process increases the time and labour costs. Although ratiometric quantitative SERS analysis offers an alternative way to improve the reliability of the quantification SERS analysis through deformation of spectral bands, which are provided by the reaction between the target analyte and Raman reporters, it is tricky and unrealistic to construct numerous appropriate SERS probes for every analyte of interest. The use of an internal standard (IS) can solve the above problem. Ren's group developed core-IS molecule-shell (CMS) nanoparticles to correct the signal fluctuation and protect the IS molecule from the interference of the external environment.[79] Nevertheless, the introduction of IS itself will bring about the inaccurate signal when the IS molecules immobilized on the surface of enhanced substrates by coordinate or electrostatic interactions do not enter the hot spot during signal acquisition. Furthermore, CMS nanostructures are complicated to synthesize, and controlling the IS molecules is not a facile process.

Based on the present deficiencies in SERS detection and quantification, Li and colleagues developed ultrathin core–shell Au@PB NPs with the characteristic Raman vibrational band at 2155 cm^{-1}, in which PB is used as the IS to improve the accuracy and reliability of quantification SERS analysis.[80] The characteristic PB spectral band in the Raman silent region significantly reduced the signal overlap and interference caused by analyte signals, and is thus suitable for use as an IS for quantitative SERS analysis in complex systems. These core–shell Au@PB NPs were applied to detect the concentrations of crystal violet (CV) in lake water and the concentrations of dopamine (DA) in blood serum without any pretreatment. It was demonstrated that the accuracy of CV and DA quantification detection
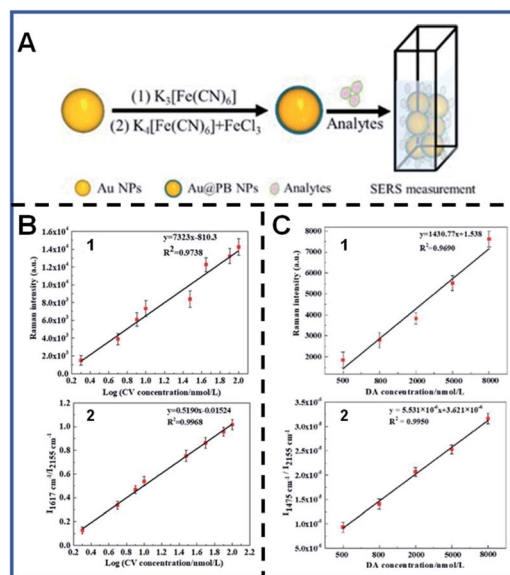

Fig. 3 Schematic showing the synthesis of Au@PB NPs for SERS quantitative analysis (A) and the calibration curves of CV (B) and DA (C). (B.1 and B.2) Calibration plot based on the $I_{1617\ \mathrm{cm}^{-1}}$ vs. log[CV] and $I_{1617\ \mathrm{cm}^{-1}}/I_{2155\ \mathrm{cm}^{-1}}$ vs. log[CV], respectively. (C.1 and C.2) Calibration plot based on $I_{1475\ \mathrm{cm}^{-1}}$ vs. [DA] and $I_{1475\ \mathrm{cm}^{-1}}/I_{2155\ \mathrm{cm}^{-1}}$ vs. [DA]. Reproduced with permission from ref. 80. Copyright 2019 American Chemical Society.

was effectively improved with the coefficient of determination of CV quantification detection increasing from 0.9738 to 0.9968 and that of DA quantification detection increasing from 0.9690 to 0.9950. Li's group also demonstrated that Au@PB NPs remain stable in different pH and temperature conditions, and are thus feasible for the detection of practical samples[80] (Fig. 3). Lu's group synthesized stable Au@PB@Au NPs and employed them for trace detection of Interleukin-6 (IL-6) in plasma. PB is used as IS molecules and is further protected by Au shell, significantly improving the linearity of IL-6 detection.[81]

Dynamic quantification detection of intracellular local pH has been successfully achieved by several groups based on the pH-dependent SERS spectra of some Raman reporters, such as MBA,[82,83] 2-aminobenzenethiol (2-ABT),[84,85] or 4-mercaptopyridine (4-MPy).[86,87] It was refreshing that a PB-caged pH-responsive SERS probe was designed by Liu's group with 4-MPy as the pH-responsive molecule.[88] This pH-responsive probe can provide an excellent response toward pH, even in the presence of many disturbances, such as human serum albumin (HSA), glutathione (GSH) and cell culture medium. Fig. 4 shows the typical pH imaging for intracellular pH monitoring under the diverse conditions in living HeLa cells using this PB-caged pH-responsive SERS probe. The obtained Raman band at 2138 cm^{-1} of PB can be employed to ascertain the probe distribution with high accuracy. Furthermore, the changes in the intensity at 1594 cm^{-1} and 1614 cm^{-1} ($I_{1594\ \mathrm{cm}^{-1}}/I_{1614\ \mathrm{cm}^{-1}}$) were employed for the pH variation quantification, showing the ability of this novel probe for the statistical analyses of intracellular pH. More importantly, the PB-caged strategy also has potential for simultaneous nanodrug transport and tumour
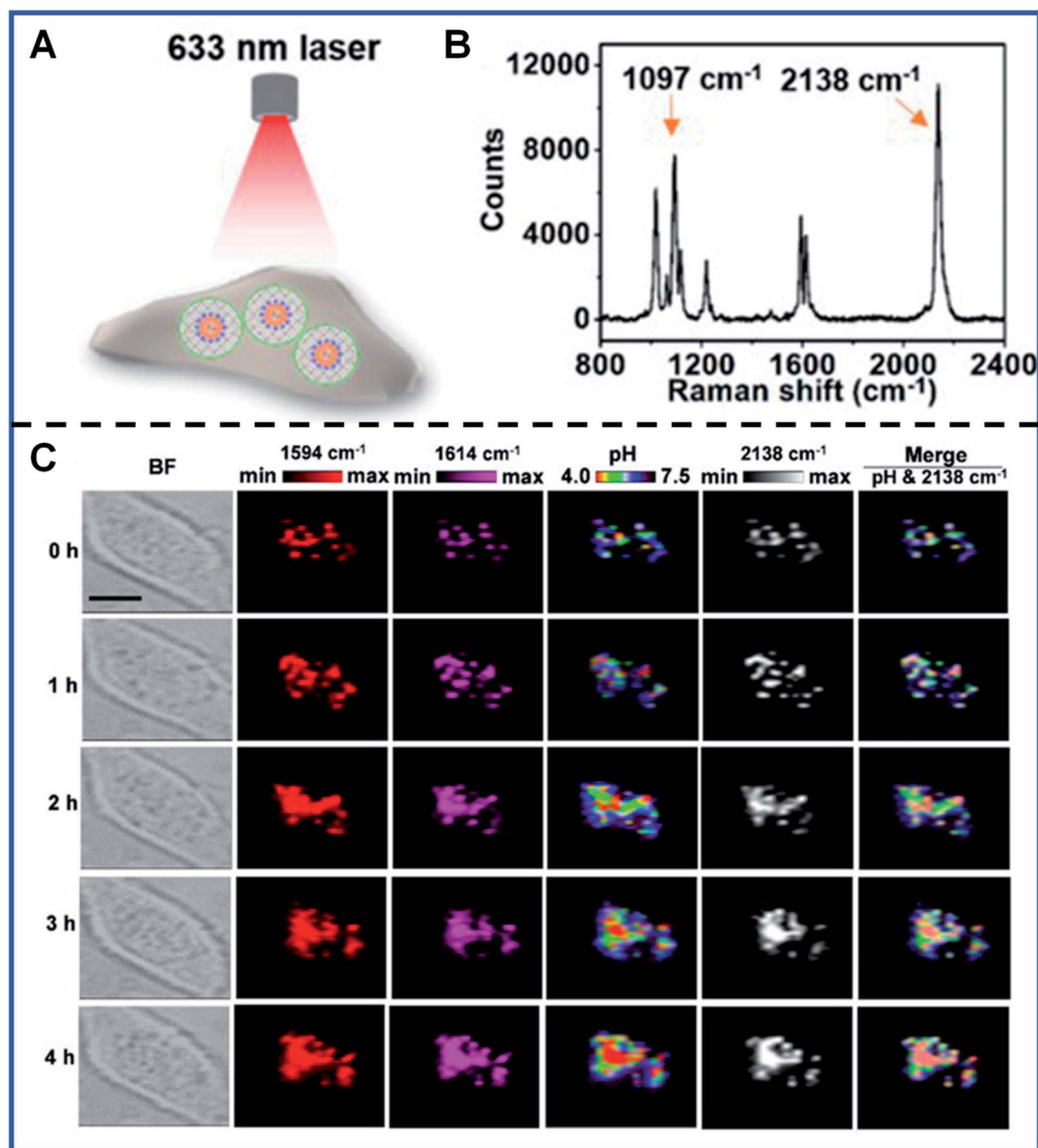
Fig. 4 Intracellular pH monitoring using PB-caged 4-MPy-Au NPs as the pH probe. (A) A schematic illustrating the profiling of intracellular probes carried out with a 633 nm laser. (B) Raman spectrum showing the characteristic Raman band of pH probes in PBS. (C) Real-time imaging of a single cell at different times using PB-caged 4-MPy-Au NPs as the pH probe. Reproduced with permission from ref. 88. Copyright 2020 American Chemical Society.

detection in biomedical applications. Even though great progress has been made for improving the reliability of quantitative SERS analysis, further advances in quantitative SERS bioanalysis will be promoted by better design strategies, such as the combination of the solid SERS substrates and PB-based nanoparticles, which guarantee a reproducible number of Raman reporters in the hot spots. The batch preparation route with good repeatability for synthesizing NPs with uniform size and morphology will also be a creative endeavour in the future.

3.2. Multispectral bioanalysis

Multi-colour imaging has attracted more and more attention for satisfying the increased demand for intracellular multi-

component analysis with the rapid development of life analytical chemistry. Developing novel multi-colour imaging methods and probes is essential to the better understanding of the various intracellular activities such as intracellular molecule interactions, intercellular communication, and the molecular changes during the production process of cancer. PB-based SERS tags have the potential to be used as multi-signal output due to their narrow peak width and adjustable Raman shift. Therefore, PB-based SERS tags have aroused extensive interest for their employment in biological multi-colour analysis and imaging.

Shen's group performed a series of pioneering studies on encoding the Raman intensities and Raman shifts of PB-based SERS tags in multispectral bioanalysis. They designed three
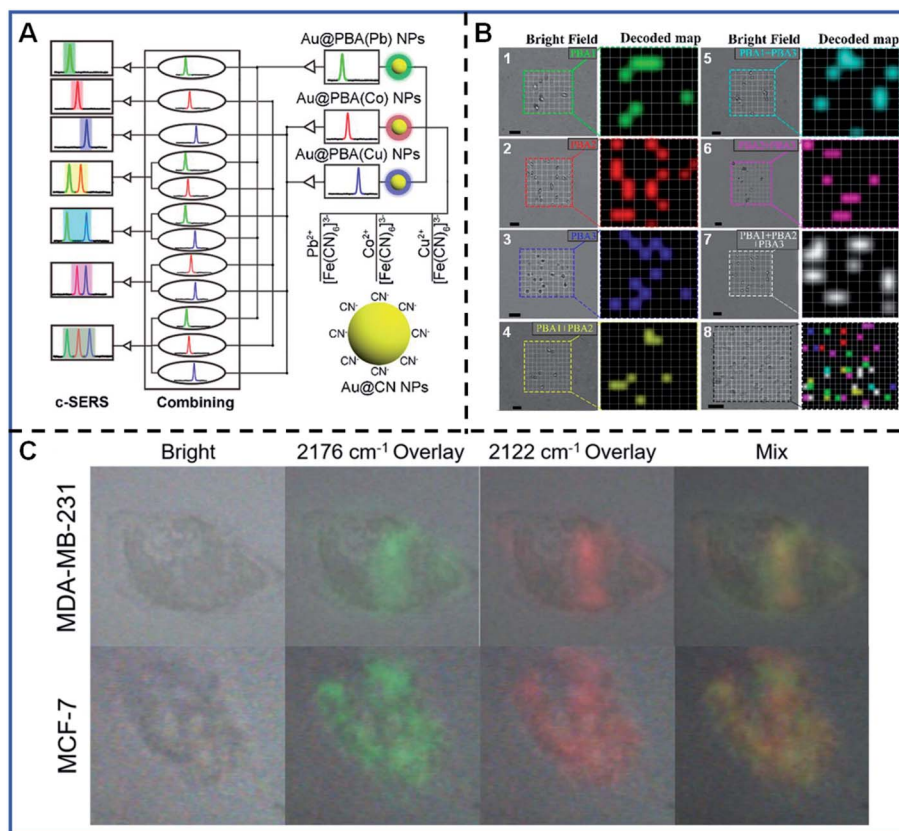
Fig. 5 The multispectral analysis of bacteria recognition and cancer cell subtyping. (A) Schematic illustrating the conception of the c–SERS. Adapted with permission from ref. 89. Copyright 2019 American Chemical Society. (B) Decoding and spatial visualization of various bacteria based on the c-SERS. B.1–B.7 corresponds to four types of bacteria, including *Escherichia coli*, *Staphylococcus aureus*, *Pseudomonas aeruginosa*, and *Bacillus cereus*. B.8 represents the simultaneous detection of various bacteria. Adapted with permission from ref. 89. Copyright 2019 American Chemical Society. (C) Simultaneous Raman imaging of two kinds of cancer cells. Adapted with permission from ref. 62. Copyright 2021 Elsevier.

Au@PBA NPs with distinguishable Raman shifts in the bio-silent region by replacing the Fe^{2+}/Fe^{3+} with other metal ions, including Au@PBA (Pb) NPs, Au@PBA (Co) NPs and Au@PBA (Cu) NPs. Based on three Au@PBA nanomaterials, they proposed combined SERS (c-SERS) and applied it in the high-throughput detection of micrometre-scale objects, such as bacteria.[89] The c-SERS output involves the various combination of independent SERS signal outputs from three PBA-encoded SERS tags, which were obtained when three Au@PBA NPs were confined in a micron-scale object. As shown in Fig. 5A, seven kinds of SERS signal outputs can be obtained with this encoding strategy, thus seven diverse micro-scale analytes can be recognized in a single detection. They demonstrated the simultaneous recognition of seven types of bacteria based on the "ID" information provided by the diverse combination of SERS tags (Fig. 5B). Through primary decoding, C-SERS could simultaneously realize the high-throughput labelling of $(2n-1)$ various micro-scale targets with only n distinguishing SERS tags, which greatly expanded the capacity of optical labels.

Apart from the c-SERS strategy, the Raman intensity difference of PB-based SERS tags caused by the marker expression difference is also an essential indicator for the accurate recognition of cell subtyping. Shen's group substantiated the conclusion by the fine synthesis of Au@PBA (Pb) NPs and Au@PBA (Cu) NPs.[62]
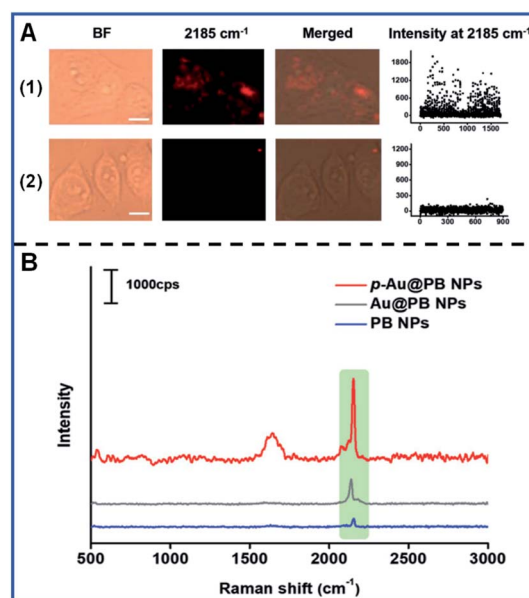

Fig. 6 The Raman mapping of multiple cancer cells (A) and the Raman spectra of different NPs (B). (A.1) The Raman mapping of HeLa cells with the upregulation of FA receptors. (A.2) The Raman mapping of HepG2 cells with the downregulation of FA receptors. Reproduced with permission from ref. 63. Copyright 2019 John Wiley & Sons, Inc.

Fig. 5C shows the different cell marker imaging of MCF-7 and MDA-MB-231 cell lines by simultaneously incubating two kinds of cell lines with two kinds of Au@PBA NPS. MCF-7 and MDA-MB-231 were able to be discriminated by the ratio of the average Raman intensities at 2176 cm^{-1} and the average Raman intensities at 2122 cm^{-1} ($I_{2176 \text{ cm}^{-1}}/I_{2122 \text{ cm}^{-1}}$), which correspond to the expression of the epidermal growth factor receptor (EGFR) and epithelial cell adhesion molecule (EpCAM), respectively. This kind of multi-colour imaging has great potential for cancer cell diagnosis and is likely to promote profiling advances in cancer cell subtypes.

3.3. Cell-imaging joint phototherapy

The SERS technique is advantageous in live-cell imaging due to the following. First, high sensitivity can be achieved with low laser power, thus avoiding light-induced injury to the cells. Second, the Raman signal of water is fairly weak, satisfying the detection requirement of the bio-environment. Third, the production process of Raman scattering and the data acquisition are relatively short, enabling real-time and long-time monitoring of biological processes. PB-based SERS tags are increasingly being used in living cell studies due to their low toxicity, excellent biocompatibility, strong and sharp Raman bands.

A vital application of PB-based SERS tags in living cells is the detection of cancer biomarkers or bacteria, demonstrating their excellent capacity for high-throughput identification of cancer cells and bacteria. Yin *et al.* synthesized Au@PB NPs in which PB was used as a background-free Raman reporter. After surface modification with targeting molecules, the FA-conjugated
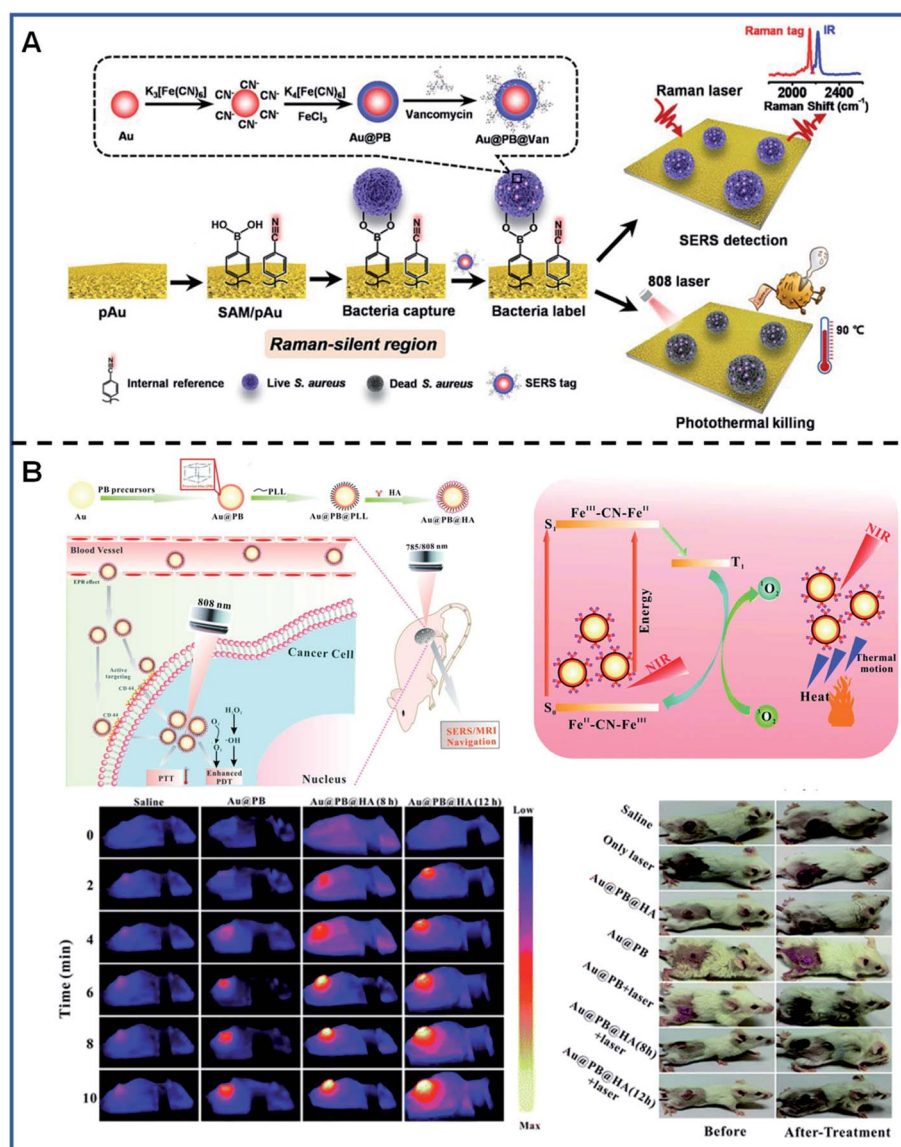

Fig. 7 Bacteria detection and tumour location using PB-based SERS tags. (A) A schematic illustrating the detection and elimination process of bacteria. Adapted with permission from ref. 61. Copyright 2021 American Chemical Society. (B) The detection and phototherapy of tumours *in vivo*. Reproduced from ref. 65 with permission from Royal Society of Chemistry. Copyright 2020 Royal Society of Chemistry.

Au@PB NPs were used to recognize the FA receptor overexpressed in HeLa cells.[50]

Similarly, Li and colleagues developed FA-conjugated p-Au@PB NPs to recognize the FA receptor overexpressed in HeLa cells and downregulation in HepG2 cells (Fig. 6A).[63] The Raman intensity of p-Au@PB NPs is largely stronger than that of Au@PB NPs and PB NPs under the same conditions (Fig. 6B), showing the potential of p-Au@PB NPs for higher detection sensitivity.

An interesting and novel integrated SERS platform for reliable detection and the photothermal elimination of bacteria was reported.[61] As shown in Fig. 7A, a wormlike plasmonic gold film with 4-mercaptophenylboronic acid (4-MPBA) and 4-mercaptobenzonitrile (4-MBN) was prepared, in which 4-MPBA was used to capture the bacteria and 4-MBN was used as the IS molecule. Additionally, vancomycin-modified core–shell Au@PB NPs (Au@PB@Van NPs) were used as the SERS tags. Therefore, both reliable quantification detection based on the statistical analysis of the imaging of bacteria and *in situ* photothermal elimination of bacteria with the 808 nm laser irradiation can be simultaneously achieved in whole blood samples.

In vivo SERS imaging plays an essential role in the tracking of the existence and location of tumours and, therefore, has the potential to be used for guiding surgical tumour removal. SERS/MR bimodal imaging has been employed for dendritic cell (DC) activation and tracking by using gadolinium-doped Au@PB NPs as bimodal agents.[64] Gd^{3+} was doped into the PB shells by replacing the $FeCl_3$ solution with the mixture of $FeCl_3$ and $GdCl_3$ in order to obtain a better MR imaging ability. SERS/MR bimodal imaging opens up a promising means for activating and tracking DC. Furthermore, SERS/MR dual-mode imaging has also been used for the guidance of both tumour localization and *in situ* PT/PD treatment using hyaluronic acid (HA)-conjugated Au@PB NPs as targeting theragnostic agents. During the process of treatment, Au@PB NPs showed a decent photothermal effect. Furthermore, PB can stimulate the generation of $^1O_2$ based on the molecular oxygen present in the surrounding environment using the 808 nm laser irradiation, contributing to the effective treatment of tumours in the mice (Fig. 7B).[65]

Although PB-based SERS nanotags have exhibited outstanding advantages for photothermal therapy and have improved the quantitative accuracy, it is noted that there is the potential for photodamage to normal cells during the cell imaging process, thus it is essential to improve the specific targeting of the nanotags to the abnormal cells. On the other hand, photodamage is usually caused by high-power lasers and long irradiation times, so it is also urgent to increase the brightness of PB-based SERS tags and design PB-based SERS tags suitable for longer-wavelength lasers. Moreover, further exploration should be carried out to improve the long-term stability of PB-based SERS nanotags for their wide biological applications.

4. Summary and outlook

This review provides a comprehensive summary of PB-based SERS tags and their biological applications. PB-based SERS tags have been synthesized as newly emerging optical nanoprobes consisting of Au NPs, PB or PBA, and functional moieties. Compared with the commonly-used Raman reporter molecules, PB and PBA are powerful competitors as Raman reporters, which provide a distinguished Raman band and avoid the competitive adsorption between analytes and Raman reporters. Moreover, PB possesses the advantages of low toxicity, satisfying the requirement in biological analysis, and PB has been demonstrated as a novel class of MR contrast agent due to the presence of iron ions. PB-based SERS tags have been investigated for the quantification analysis of key molecules highly related to human health as well as the recognition of microscale objects such as bacteria and cancer cells. The multifunctional detection platform can be constructed by fine-tuning the various components of the PB-based SERS tag. Even so, all these current studies remain in the early stages for the development of SERS techniques as clinically available means of diagnosis.

Previous studies of PB-based SERS tags will help to navigate future development. However, there are still many challenges to be overcome in the field before PB-based SERS tags can be used as commercial nanoprobes to answer significant biomedical questions. The reliability of indirect SERS bioanalysis is decided by both the reproducible preparation and the stability of SERS tags; therefore, the delicate control of the preparation conditions, including a more mature and replicable approach and the further protection with the surfactant, is critical for synthesizing stable and uniform PB-based SERS tags. Moreover, breakthroughs in the femtosecond time scale and nanometre resolution are possible, combined with the application of ultrafast lasers and the development of high spatial resolution techniques such as tip-enhanced Raman scattering (TERS).[90,91] With the development and popularity of portable Raman,[92,93] SERS techniques with PB-based SERS tags will be a promising tool for point of care (POC) pathogen diagnosis and molecular detection.

Diversified design is another developing orientation of PB-based SERS tags. The gadolinium-doped strategies provide a new perspective for the biomedical application of PB-based SERS tags. For instance, the PB-based SERS tags have the potential to promote wound healing by doping with calcium ions or zinc ions. The fine-tuning of the morphology of the PB shell, such as the caged PB shell, can also be used as the nanodrug carrier for the treatment of tumours and cancer. Additionally, PB-based SERS tags provide much information for *in vivo* tumour location, thereby assisting with the selective removal of tumour tissue from the damaged tissue. When combined with the 808 nm laser irradiation, the prognosis after surgery will be significantly improved. Although there is still much work to be done using PB-based SERS tags for the reliable quantitative measurements in complex biosystems and the surgery guidance combined with the treatment in the biomedical area, we can still look forward to the increased SERS-based practical applications along with further development of portable instruments and the preparation method of PB-based SERS tags.

Notably, PB is regarded as one of the metal–organic frameworks (MOFs), indicating the potential of MOF for constructing

SERS nanotags used in SERS detection. MOFs, as highly porous crystalline materials, have rapidly attracted great interest in the emerging MOF-SERS field due to their nanoporous functionality, large surface area, excellent dispersibility, and designable functions. Recently, different MOFs have been used to stabilize noble metal nanoparticles and adsorb analyte molecules in close proximity to the "hotspots", improving the detection reproducibility and sensitivity of SERS application. MOFs have been applied in SERS detection in multiple areas, such as environmental analysis,[94–96] food safety,[97–99] bio-medicine[100,101] and real-time monitoring.[102,103] In the future, the introduction of more novel MOF materials or the modification of MOF materials for constructing SERS tags will further extend the reliable application of SERS.

Conflicts of interest

There are no conflicts to declare.

Acknowledgements

Notes and references

1 P. A. Mosier-Boss, *Nanomaterials*, 2017, **7**, 142.

2 J. Perumal, Y. Wang, A. B. E. Attia, U. S. Dinish and M. Olivo, *Nanoscale*, 2021, **13**, 553.

3 J. Sun, L. Gong, W. Wang, Z. Gong, D. Wang and M. Fan, *Luminescence*, 2020, **35**, 808.

4 K. Kneipp, Y. Wang, H. Kneipp, L. T. Pe, I. Itzkan, R. R. Dasarirelman and M. S. Feld, *Phys. Rev. Lett.*, 1997, **78**, 1667.

5 S. M. Stranahan and K. A. Willets, *Nano Lett.*, 2010, **10**, 3777.

6 J. P. Camden, J. A. Dieringer, Y. Wang, D. J. Masiello, L. D. Marks, G. C. Schatz and R. P. Van Duyne, *J. Am. Chem. Soc.*, 2008, **130**, 12616.

7 Z. Zheng, S. Cong, W. Gong, J. Xuan, G. Li, W. Lu, F. Geng and Z. Zhao, *Nat. Commun.*, 2017, **8**, 1993.

8 P. K. Kannan, P. Shankar, C. Blackman and C. H. Chung, *Adv. Mater.*, 2019, **31**, 1803432.

9 R. A. Alvarez-Puebla and L. M. Liz-Marzan, *Chem. Soc. Rev.*, 2012, **41**, 43.

10 D. Li, D. M. Yao, C. N. Li, Y. H. Luo, A. H. Liang, G. Q. Wen and Z. l. Jiang, *TrAC, Trends Anal. Chem.*, 2020, **127**, 115885.

11 M. Fan, G. F. S. Andrade and A. G. Brolo, *Anal. Chim. Acta*, 2020, **1097**, 1.

12 S. A. Ogundare and W. E. van Zyl, *Cellulose*, 2019, **26**, 6489.

13 H. K. Lee, Y. H. Lee, C. S. L. Koh, G. C. Phan-Quang, X. Han, C. L. Lay, H. Y. F. Sim, Y. C. Kao, Q. An and X. Y. Ling, *Chem. Soc. Rev.*, 2019, **48**, 731.

14 F. S. Flores, E. Méndez, M. L. Castaños, A. C. Lima, K. A. L. Castaños, M. A. G. Fuentes and A. M. Albores, *Biosensors*, 2021, **11**, 66.

15 M. Sarah, F. Karen and G. Duncan, *J. Photochem. Photobiol., C*, 2014, **21**, 40.

16 Y. Zeng, K. M. Koo, M. Trau, A. G. Shen and J. M. Hu, *Appl. Mater. Today*, 2019, **15**, 431.

17 X. S. Zheng, I. J. Jahn, K. Weber, D. Cialla-May and J. Popp, *Spectrochim. Acta, Part A*, 2018, **197**, 56.

18 Y. C. Song, T. L. Xu, L. P. Xu and X. J. Zhang, *Nanoscale*, 2018, **10**, 20990.

19 B. Han, Y. L. Zhang, L. Zhu, X. H. Chen, Z. C. Ma, X. L. Zhang, J. N. Wang, W. Wang, Y. Q. Liu, Q. D. Chen and H. B. Sun, *Sens. Actuators, B*, 2018, **270**, 500.

20 E. Garcia-Rico, R. A. Alvarez-Puebla and L. Guerrini, *Chem. Soc. Rev.*, 2018, **47**, 4909.

21 J. Ma, G. Feng, Y. Ying, Y. Shao, Y. She, L. Zheng, A. M. Abd Ei-Aty and J. Wang, *Analyst*, 2021, **146**, 956.

22 W. Fan, S. Yang, Y. Zhang, B. Huang, Z. Gong, D. Wang and M. Fan, *ACS Sens.*, 2020, **5**, 3599.

23 A. Teixeira, J. L. Paris, F. Roumani, L. Dieguez, M. Prado, B. Espina, S. Abalde-Cela, A. Garrido-Maestu and L. Rodriguez-Lorenzo, *Materials*, 2020, **13**, 1934.

24 J. Langer, I. Garcia and L. M. Liz-Marzan, *Faraday Discuss.*, 2017, **205**, 363.

25 Y. Wang, S. Zong, N. Li, Z. Wang, B. Chen and Y. Cui, *Nanoscale*, 2019, **11**, 2460.

26 Y. Liu, S. Yue, Y. N. Wang, Y. Wang and Z. R. Xu, *Sens. Actuators, B*, 2020, **310**, 127889.

27 S. Yue, X. Sun, N. Wang, Y. Wang, Y. Wang, Z. Xu, M. Chen and J. Wang, *ACS Appl. Mater. Interfaces*, 2017, **9**, 39699.

28 Y. Wang, B. Yan and L. Chen, *Chem. Rev.*, 2013, **113**, 1391.

29 L. Fabris, *J. Opt.*, 2015, **17**, 114002.

30 S. Cheng, B. Zheng, D. B. Yao, Y. Wang, J. J. Tian, L. H. Liu, H. J. Liang and Y. S. Ding, *Anal. Lett.*, 2019, **52**, 902.

31 T. T. B. Quyen, C. C. Chang, W. N. Su, Y. H. Uen, C. J. Pan, J. Y. Liu, J. Rick, K. Y. Lin and B. J. Hwang, *J. Mater. Chem. B*, 2014, **2**, 629.

32 N. Choi, H. Dang, A. Das, M. S. Sim, I. Y. Chung and J. Choo, *Biosens. Bioelectron.*, 2020, **164**, 112326.

33 J. He, Y. Qiao, H. Zhang, J. Zhao, W. Li, T. Xie, D. Zhong, Q. Wei, S. Hua, Y. Yu, K. Yao, H. A. Santos and M. Zhou, *Biomaterials*, 2020, **234**, 119763.

34 Y. Feng, L. He, L. Wang, R. Mo, C. Zhou, P. Hong and C. Li, *Nanomaterials*, 2020, **10**, 1000.

35 L. Sun, Z. L. Yu and M. S. Lin, *Analyst*, 2019, **144**, 4820.

36 L. Lin, H. Gu and J. Ye, *Chem. Commun.*, 2015, **51**, 17740.

37 Y. Zeng, J. Q. Ren, A. G. Shen and J. M. Hu, *J. Am. Chem. Soc.*, 2018, **140**, 10649.

38 Y. T. Shen, L. J. Liang, J. Zhang, Z. Y. Li, J. Yue, J. Q. Wang, W. Q. Xu, W. Shi and S. P. Xu, *Sens. Actuators, B*, 2019, **285**, 84.

39 A. G. Shen, L. F. Chen, W. Xie, J. C. Hu, A. Zeng, R. Richards and J. M. Hu, *Adv. Funct. Mater.*, 2010, **20**, 969.

40 J. Li, H. Liu, P. Rong, W. Zhou, X. Gao and D. Liu, *Nanoscale*, 2018, **10**, 8292.

41 J. L. Gong, J. H. Jiang, H. F. Yang, G. L. Shen, R. Q. Yu and Y. Ozaki, *Anal. Chim. Acta*, 2006, **564**, 151.

42 N. G. Khlebtsov, L. Lin, B. N. Khlebtsov and J. Ye, *Theranostics*, 2020, **10**, 2067.

43 S. Sloan-Dennison, M. R. Bevins, B. T. Scarpitti, V. K. Sauve and Z. D. Schultz, *Analyst*, 2019, **144**, 5538.

44 Y. Shen, J. Yue, W. Shi, W. Xu and S. Xu, *Biosens. Bioelectron.*, 2020, **151**, 111957.

45 X. W. Wang and L. Cheng, *Coord. Chem. Rev.*, 2020, **419**, 213393.

46 M. A. Busquets and J. Estelrich, *Drug Discovery Today*, 2020, **25**, 1431.

47 Z. Qin, Y. Li and N. Gu, *Adv. Healthcare Mater.*, 2018, **7**, e1800347.

48 S. F. A. Kettle, E. Diana, E. M. C. Marchese, E. Boccaleri and P. L. Stanghellini, *J. Raman Spectrosc.*, 2011, **42**, 2006.

49 G. Moretti and C. Gervais, *J. Raman Spectrosc.*, 2018, **49**, 1198.

50 Y. Yin, Q. Li, S. Ma, H. Liu, B. Dong, J. Yang and D. Liu, *Anal. Chem.*, 2017, **89**, 1551.

51 E. Lenzi, D. J. D. Aberasturi and L. M. Liz-Marzan, *ACS Sens.*, 2019, **4**, 1126.

52 M. Muhammad and Q. Huang, *Talanta*, 2021, **227**, 122188.

53 J. Xu, C. Li, H. Si, X. Zhao, L. Wang, S. Jiang, D. Wei, J. Yu, X. Xiu and C. Zhang, *Opt. Express*, 2018, **26**, 21546.

54 J. Guo, X. Yan, M. Xu, G. Ghimire, X. Pan and J. He, *Anal. Chem.*, 2021, **93**, 4441.

55 R. X. He, R. Liang, P. Peng and Y. Norman Zhou, *J. Nanopart. Res.*, 2017, **19**, 1.

56 C. Hu, J. Shen, J. Yan, J. Zhong, W. Qin, R. Liu, A. Aldalbahi, X. Zuo, S. Song, C. Fan and D. He, *Nanoscale*, 2016, **8**, 2090.

57 M. Zannotti, A. Rossi and R. Giovannetti, *Coatings*, 2020, **10**, 288.

58 A. Y. F. Mahmoud, C. J. Rusin and M. T. McDermott, *Analyst*, 2020, **145**, 1396.

59 K. Li, G. Liu, S. Zhang, Y. Dai, S. Ghafoor, W. Huang, Z. Zu and Y. Lu, *Nanoscale*, 2019, **11**, 9587.

60 P. Sha, Q. Su, P. Dong, T. Wang, C. Zhu, W. Gao and X. Wu, *RSC Adv.*, 2021, **11**, 27107.

61 X. Gao, Y. Yin, H. Wu, Z. Hao, J. Li, S. Wang and Y. Liu, *Anal. Chem.*, 2021, **93**, 1569.

62 Y. M. Shen, M. Y. Gao, X. Chen, A. G. Shen and J. M. Hu, *Spectrochim. Acta, Part A*, 2021, **252**, 119566.

63 X. Li, E. Zeng, H. Di, Q. Li, J. Ji, J. Yang and D. Liu, *Adv. Biosyst.*, 2019, **3**, e1900046.

64 C. Zhang, Z. Xu, H. Di, E. Zeng, Y. Jiang and D. Liu, *Theranostics*, 2020, **10**, 6061.

65 W. Zhu, M. Y. Gao, Q. Zhu, B. Chi, L. W. Zeng, J. M. Hu and A. G. Shen, *Nanoscale*, 2020, **12**, 3292.

66 J. Li, J. Wang, Y. S. Grewal, C. B. Howard, L. J. Raftery, S. Mahler, Y. Wang and M. Trau, *Anal. Chem.*, 2018, **90**, 10377.

67 M. Arabi, A. Ostovan, Z. Zhang, Y. Wang, R. Mei, L. Fu, X. Wang, J. Ma and L. Chen, *Biosens. Bioelectron.*, 2021, **174**, 112825.

68 X. Wang, N. Choi, Z. Cheng, J. Ko, L. Chen and J. Choo, *Anal. Chem.*, 2017, **89**, 1163.

69 S. Ganesh, K. Venkatakrishnan and B. Tan, *Nat. Commun.*, 2020, **11**, 1135.

70 J. Plou, I. García, M. Charconnet, I. Astobiza, C. García-Astrain, C. Matricardi, A. Mihi, A. Carracedo and L. M. Liz-Marzán, *Adv. Funct. Mater.*, 2020, **30**, 1910335.

71 J. Kelly, R. Patrick, S. Patrick and S. E. J. Bell, *Angew. Chem. Int. Ed.*, 2018, **57**, 15686.

72 J. Guo, A. Sesena Rubfiaro, Y. Lai, J. Moscoso, F. Chen, Y. Liu, X. Wang and J. He, *Analyst*, 2020, **145**, 4852.

73 G. H. Yang, Q. Zhang, Y. Liang, H. Liu, L. L. Qu and H. T. Li, *Colloids Surf., A*, 2019, **562**, 289.

74 M. N. Sanz-Ortiz, K. Sentosun, S. Bals and L. M. Liz-Marzán, *ACS Nano*, 2015, **9**, 10489.

75 F. Yu, M. Su, L. Tian, H. Wang and H. Liu, *Anal. Chem.*, 2018, **90**, 5232.

76 L. Liu, C. J. Shangguan, J. L. Guo, K. J. Ma, S. L. Jiao, Y. Yao and J. Q. Wang, *Adv. Opt. Mater.*, 2020, **8**, 2001214.

77 X. Qin, Y. Si, D. Wang, Z. Wu, J. Li and Y. Yin, *Anal. Chem.*, 2019, **91**, 4529.

78 J. Chen, Y. Wu, C. Fu, H. Cao, X. Tan, W. Shi and Z. Wu, *Biosens. Bioelectron.*, 2019, **143**, 111619.

79 W. Shen, X. Lin, C. Y. Jiang, C. Y. Li, H. X. Lin, J. T. Huang, S. Wang, G. K. Liu, X. M. Yan, Q. L. Zhong and B. Ren, *Angew. Chem. Int. Ed.*, 2015, **54**, 7308.

80 M. Li, J. Y. Wang, Q. Q. Chen, L. H. Lin, P. Radjenovic, H. Zhang, S. Y. Luo, Z. Q. Tian and J. F. Li, *Anal. Chem.*, 2019, 15025.

81 T. Zhou, D. Lu, Q. She, C. Chen, J. Chen, Z. Huang, S. Feng, R. You and Y. Lu, *Sens. Actuators, B*, 2021, **336**, 129597.

82 F. Sun, P. Zhang, T. Bai, D. D. Galvan, H. C. Hung, N. Zhou, S. Y. Jiang and Q. M. Yu, *Biosens. Bioelectron.*, 2015, **73**, 202.

83 H. Wei, M. R. Willner, L. C. Marr and P. J. Vikesland, *Analyst*, 2016, **141**, 5159.

84 Y. Shen, L. Liang, S. Zhang, D. Huang, J. Zhang, S. Xu, C. Liang and W. Xu, *Nanoscale*, 2018, **10**, 1622.

85 Y. T. Huang, W. Liu, D. M. Wang, Z. J. Gong and M. K. Fan, *Microchem. J.*, 2020, **154**, 104565.

86 G. Zhu, L. Cheng, G. Liu and L. Zhu, *Nanomaterials*, 2020, **10**, 1501.

87 A. Quinn, Y. H. You and M. J. McShane, *Sensors*, 2019, **19**, 3521.

88 Y. Bi, H. Di, E. Zeng, Q. Li, W. Li, J. Yang and D. Liu, *Anal. Chem.*, 2020, **92**, 9574.

89 M. Y. Gao, Q. Chen, W. Li, A. G. Shen and J. M. Hu, *Anal. Chem.*, 2019, **91**, 13866.

90 B. Pettinger, B. Ren, G. Picardi, R. Schuster and G. Ertl, *J. Raman Spectrosc.*, 2005, **36**, 541.

91 B. R. Wood, E. Bailo, M. A. Khiavi, L. Tilley, S. Deed, T. Deckert-Gaudig, D. McNaughton and V. Deckert, *Nano Lett.*, 2011, **11**, 1868.

92 X. Gong, M. Tang, Z. Gong, Z. Qiu, D. Wang and M. Fan, *Food Chem.*, 2019, **295**, 254.

93 W. Zhu, B. Y. Wen, L. J. Jie, X. D. Tian, Z. L. Yang, P. M. Radjenovic, S. Y. Luo, Z. Q. Tian and J. F. Li, *Biosens. Bioelectron.*, 2020, **154**, 112067.

94 O. Guselnikova, P. Postnikov, R. Elashnikov, E. Miliutina, V. Svorcik and O. Lyutakov, *Anal. Chim. Acta*, 2019, **1068**, 70.

95 D. Li, X. K. Cao, Q. M. Zhang, X. G. Ren, L. Jiang, D. W. Li, W. Deng and H. T. Liu, *J. Mater. Chem. A*, 2019, **7**, 14108.

96 Q. Z. Wang, Z. H. Xu, Y. J. Zhao, S. H. Zhang, T. Bu, C. Q. Zhang, X. Wang and L. Wang, *Sens. Actuators, B*, 2021, **329**, 129080.

97 X. Zhou, G. Liu, H. Zhang, Y. Li and W. Cai, *J. Hazard. Mater.*, 2019, **368**, 429.

98 H. S. Lai, G. K. Li, F. G. Xu and Z. M. Zhang, *J. Mater. Chem. C*, 2020, **8**, 2952.

99 Q. Q. Li, S. S. Gong, H. Zhang, F. Z. Huang, L. N. Zhang and S. K. Li, *Chem. Eng. J.*, 2019, **371**, 26.

100 P. Jiang, Y. Hu and G. Li, *Talanta*, 2019, **200**, 212.

101 X. Qiao, B. Su, C. Liu, Q. Song, D. Luo, G. Mo and T. Wang, *Adv. Mater.*, 2018, **30**, 1702275.

102 S. Choi, H. J. Lee and M. Oh, *Small*, 2016, **12**, 2425.

103 Q. Xu, W. Liu, L. Li, F. Zhou, J. Zhou and Y. Tian, *Chem. Commun.*, 2017, **53**, 1880.